Published in final edited form as:
Eur J Neurosci. 2012 November ; 36(10): 3322–3332. doi:10.1111/j.1460-9568.2012.08255.x.

Functional properties of dopamine neurons and co-expression of vasoactive intestinal polypeptide in the dorsal raphe nucleus and ventro-lateral periaqueductal grey

Antonios G. Dougalis[#1], **Gillian A. C. Matthews**[#1], **Matthew W. Bishop**[1], **Frédéric Brischoux**[1,†], **Kazuto Kobayashi**[2], and **Mark A. Ungless**[1]

[1]Medical Research Council Clinical Sciences Centre, Imperial College London, Hammersmith Hospital, Du Cane Road, London W12 0NN, UK

[2]Department of Molecular Genetics, Institute of Biomedical Sciences, Fukushima Medical University School of Medicine, Fukushima 960-1295, Japan

[#] These authors contributed equally to this work.

Abstract

The dorsal raphe nucleus (DRN) and ventrolateral periaqueductal grey (vlPAG) regions contain populations of dopamine neurons, often considered to be a dorsal caudal extension of the A10 group [mostly found in the ventral tegmental area (VTA)]. Recent studies suggest they are involved in promoting wakefulness and mediate some of the antinociceptive and rewarding properties of opiates. However, little is known about their electrophysiological properties. To address this, we used Pitx3-GFP and tyrosine hydroxylase (TH)-GFP mice to carry out targeted whole-cell recordings from this population in acute brain slices. We found that DRN/vlPAG dopamine neurons have characteristics similar to most VTA dopamine neurons, but distinct from dorsal raphe serotonin neurons. They fire broad action potentials at a relatively slow, regular rate, exhibit a hyperpolarization-activated inward current and delayed repolarization, and show spike-frequency adaptation in response to prolonged depolarization. In addition, they receive fast excitatory and inhibitory synaptic inputs. Moreover, we found co-expression of vasoactive intestinal polypeptide in small, periaqueductal dopamine neurons, but generally not in larger, more ventral dopamine neurons.

Keywords

arousal; midbrain; sleep; ventral tegmental area

Correspondence: Dr M. A. Ungless, as above. mark.ungless@imperial.ac.uk.
[†]*Present address*: 'Physiopathology of the Neuronal Network Responsible for the Sleep-Waking Cycle' Team, CNRS UMR5292; INSERM U1028; Lyon Neuroscience Research Center, Lyon, F-69372, France.

The authors declare no conflicts of interest.

Introduction

The dorsal raphe nucleus (DRN) and ventrolateral periaqueductal grey (vlPAG) regions contain a small (≈1000) population of dopamine neurons, often referred to as the dorso-caudal extension of the A10 group (Hokfelt *et al.*, 1984b; Trulson *et al.*, 1985; Descarries *et al.*, 1986; Arsenault *et al.*, 1988; Stratford & Wirtshafter, 1990; Charara & Parent, 1998). Although these neurons have not been as intensively studied as other members of the A10 group [e.g. in the ventral tegmental area (VTA)], they appear to mediate some of the antinociceptive and rewarding properties of opiates (Flores *et al.*, 2004, 2006; Meyer *et al.*, 2009), suggesting that they may also play a role in processing rewards and mediating the effects of drugs of misuse, which is well established for VTA dopamine neurons (Schultz, 2002; Wise, 2004; Luscher & Ungless, 2006).

In addition, DRN/vlPAG dopamine neurons may play a role in promoting arousal and wakefulness (Lu *et al.*, 2006). For example, this population projects to, and receives inputs from, a number of regions involved in arousal and sleep, including midline and intralaminar thalamus, basal forebrain cholinergic neurons, the ventrolateral preoptic nucleus, the lateral hypothalamic orexin/hypocretin cells, the pontine latero-dorsal tegmental cholinergic cells and the locus coeruleus (Yoshida *et al.*, 1989; Stratford & Wirtshafter, 1990; Takada *et al.*, 1990; Krout *et al.*, 1998; Hasue & Shammah-Lagnado, 2002; Lu *et al.*, 2006). Moreover, DRN/vlPAG dopamine neurons express c-Fos during wakefulness, and forced wakefulness (Lu *et al.*, 2006; but see Leger *et al.*, 2010). 6-Hydroxydopamine lesions of these neurons cause a 20% increase in total sleep, which is substantial when compared with the effect of lesions in other brain regions or other specific neuronal populations (Wenk *et al.*, 1994; Hara *et al.*, 2001; Lu *et al.*, 2006), and contrasts with the limited effects on sleep of lesions of VTA dopamine neurons (Lai *et al.*, 1999; Lu *et al.*, 2006). However, whether this role for DRN/vlPAG dopamine neurons in promoting arousal is distinct from that of VTA neurons remains unclear. For example, although some *in vivo* electrophysiological recordings showed that VTA dopamine neuron firing rate is not closely related to sleep–wake states (Miller *et al.*, 1983), other reports find that they do increase burst firing during paradoxical sleep (Dahan *et al.*, 2007). Similarly, although it has been reported that c-Fos expression is increased during paradoxical sleep recovery in the VTA (Maloney *et al.*, 2002), others report no c-Fos expression following either exposure to a novel environment or paradoxical sleep recovery in the VTA (Leger *et al.*, 2010). Moreover, a subset of VTA neurons spontaneously fire only during the active phase of the diurnal cycle and may therefore promote wakefulness (Luo *et al.*, 2008), possibly driven by an indirect projection from the suprachiasmatic nucleus (Luo & Aston-Jones, 2009).

Little is known, however, about the electrophysiological properties of DRN/vlPAG dopamine neurons. For example, there is only one report of a single identified dopamine neuron in the DRN *in vivo* (Schweimer & Ungless, 2010), despite a number of single-cell labelling studies that sampled broadly in the DRN (e.g. Allers & Sharp, 2003). This may be in part because of their small size and number, which makes them difficult to find, or because they are not spontaneously active *in vivo* (which would preclude their detection with an extracellular electrode). To address this, we have used Pitx3-GFP and tyrosine

hydroxylase (TH)-GFP mice to conduct targeted whole-cell recordings in acute brain slices combined with single-cell labelling and immunohistochemistry.

Materials and methods

Brain slice preparation

Two- to 6-month-old male Pitx3-GFP (Zhao *et al.*, 2004) or TH-GFP [B6.Cg-Tg(TH-GFP)21-31/C57B6; Sawamoto *et al.*, 2001; Matsushita *et al.*, 2002] heterozygous mice were killed by isoflurane anaesthesia followed by decapitation. All breeding and experimental procedures were conducted under a project licence approved by the Home Office, in accordance with the Animals (Scientific Procedures) Act of 1986 (United Kingdom). The brain was rapidly removed out of the cranial cavity and bathed with ice-cold (0–4 °C) artificial cerebrospinal fluid (aCSF, composition in mm, NaCl 120, KCl 3.5, NaH_2PO_4 1.25, $NaHCO_3$ 25, glucose 10, $MgCl_2$ 1, $CaCl_2$ 2) fully equilibrated with carbogen gas (95% oxygen and 5% carbon dioxide). Two or three coronal brain slices (220 lm thickness) encompassing the DRN/vlPAG (bregma −4.8 to −4.2 mm) were obtained using a vibratome (Leica VT1000S; Leica Microsystems, Wetzlar, Germany) and were maintained in a standard custom-made maintenance chamber (Edwards *et al.*, 1989) gently and continuously aerated with carbogen gas for at least 90 min at room temperature (20–22 °C) before use for electrophysiology.

Electrophysiological recordings

Slices were transferred to a submersion recording chamber and were continuously perfused at a rate of 2–4 mL/min with fully oxygenated aCSF at 32 °C. Neurons were visualized using infra-red (IR) differential interference contrast (IR-DIC) under an upright microscope (BXWI 51; Olympus, Tokyo, Japan) equipped with a 40 × or 60 × objective (0.8 numerical aperture), an IR filter, DIC optics and a charge coupled device (CCD) video camera (Hamamatsu Photonics, Herrsching am Ammersee, Germany). Neurons were identified as GFP+ using fluorescence illumination (Xcite120 unit; EXFO, Eastleigh, UK) coupled to a GFP excitation filter. Putative 5HT neurons were identified as GFP), with large cell bodies, relatively slow firing rates and broad action potentials. Previous studies indicate that many, but not all, of these neurons are likely to be 5HT+ (Beck *et al.*, 2004).

Whole-cell patch-clamp recordings were performed with a Multiclamp 700B amplifier (for current-clamp and voltage-clamp; Molecular Devices, Sunnyvale, CA, USA) and an Axopatch 200A amplifier (Axon Instruments, Foster City, CA, USA; for voltage-clamp recordings) using glass microelectrodes (4–6 MΩ in resistance) filled with an internal solution containing (in m_M) 140 K-gluconate, 5 NaCl, 1 $MgCl_2$, 10 HEPES, 1 EGTA, 2 MgATP, 0.5 LiGTP and 0.1% neurobiotin (pH 7.3, osmolarity 280–290 mosmol/L. Series resistance (R_s) and input resistance (R_{in}) were frequently monitored throughout the experiments via a 10-mV, 250-ms hyperpolarizing step under voltage-clamp or through a 10- to 200-pA current injection under current-clamp (at 0.05 Hz). Any large changes in holding current or noise characteristics were taken as early signs of cell loss and recordings were terminated. Experiments were also terminated if R_s exceed 30 MΩ or if R_{in} changed more than 15% after break in the whole-cell mode. Series resistance (typical values of 10–30

MΩ) was compensated by 60–70% in the majority of the experiments. Membrane capacitance (C_m) was measured under voltage clamp at −50 mV using a hyperpolarizing 10-mV, 250-ms step. C_m was measured from the change in membrane charge taken from the integrated capacity transients (pClamp; Molecular Devices). All potentials cited here have not been corrected for liquid junction potentials (estimated using pClamp calculator as 9.2 mV for caesium-based solutions and 12.8 mV for K-gluconate).

Cells were recorded in current-clamp conditions for a minimum of 1–2 min after breaking into the whole-cell mode to establish their average resting membrane potential (V_m) and their action potential (AP) basal firing frequency before delivering hyperpolarizing/depolarizing pulses. In spontaneously active cells, AP firing frequency was calculated over 60- to 120-s epochs. The coefficient of variation of the inter-spike-interval (CV-ISI) was calculated by dividing standard deviation by the mean ISI for each cell recorded. During this period, 50–300 APs were averaged and the AP amplitude, threshold (defined as a steep change of voltage of 10 mV/ms), width at base (at the level of the threshold), as well as the afterhyperpolarisation (AHP) amplitude (given as the absolute membrane potential at the peak) and AHP rate of repolarization (during the first 10 ms after AHP peak) were measured. Instantaneous and steady-state firing frequencies of neurons in response to depolarizing current injection were calculated at the first 100 ms and last 2 s of the 5-s depolarizing step, respectively.

To determine I_h, cells were held at −50 mV in voltage-clamp mode, and 10-mV incremental hyperpolarizing steps (1000 ms in duration) were delivered to −120 mV. The amplitude of the I_h current was measured and plotted at each holding potential as the difference between the peak instantaneous (before I_h activation) and steady-state current (measured 20 ms before the end of the step as shown in Fig. 4A). We have measured the amplitude of the steady-state current after near complete activation of the I_h current during a hyperpolarizing pulse from −50 to −120 mV.

Synaptic currents were examined in voltage-clamp mode at either −70 or 0 mV to selectively monitor spontaneous excitatory post-synaptic currents (sEPSCs) or inhibitory post-synaptic currents (sIPSCs), respectively. Electrodes contained the K-gluconate solution detailed above. Three- to 5-min epochs of spontaneous activity were logged at each holding potential and the records were analysed for their frequency and amplitude using MINI ANALYSIS software (Synaptosoft; for comparison of Pitx3-GFP and p5HT neurons, detection thresholds were set to 10 pA for sEPSCs and 20 pA for sIPSCs; for comparison of VIP+ and VIP− neurons detection thresholds were set at 7 pA for sEPSCs and 15 pA for sIPSCs). For evoked events, a bipolar stimulator (FHC, Bowdoin, ME, USA) was positioned close (100–400 μm) to the recorded cell. Stimulus intensity was adjusted to evoke monosynaptic events at 40–50% intensity of the maximal evoked current resulting in recording single-peak, fast-rising, fast-decaying currents. Paired pulse experiments used an ISI of 50 ms (stimulus duration 20–100 μs, intensity 20–60 V, delivered every 30 s). The paired-pulse ratio (PPR) was calculated by dividing the average peak amplitude of the PSC generated by the second stimulus by the average peak amplitude generated by the first.

To determine AMPAR (*α*-amino-3-hydroxy-5-methyl-4-isoxazole-propionic acid receptor)/NMDAR (*N*-methyl-D-aspartate receptor) ratios, the neuron was voltage-clamped at +40 mV (in the presence of picrotoxin, 100 *μ*m) and a stable mixed AMPAR- and NMDAR-mediated EPSC was recorded. Electrodes contained an internal solution of (in mm): $CsCH_3SO_3$ 125, NaCl 2.8, HEPES 20, EGTA 0.4, TEA-Cl 5, MgATP 2, LiGTP 0.5. The NMDAR antagonist d-AP5 (50 lm) was then applied to the slice, and the pure AMPAR current recorded. This was then digitally subtracted from the mixed current using clampfit 10.2 (Molecular Devices) to give the pure NMDAR current, and an AMPAR/NMDAR ratio calculated by dividing the peak amplitude of the average AMPAR-mediated EPSC by the peak amplitude of the NMDAR-mediated EPSC. All data were low-pass filtered at 1 kHz, collected at 3–5 kHz using winwcp software (courtesy of John Dempster, University of Strathclyde, UK) or pClamp (Molecular Devices) and were stored on a personal computer for offline analysis using winwcp, clampfit 10.2 (Molecular Devices) and Spike 2 (Cambridge Electronic Design, Cambridge, UK).

All values reported here are means ± standard error of the mean (SEM). Statistical tests were *t*-tests (non-directional), anova (with Newman–Keuls *post-hoc* tests where appropriate) or chi-squared (performed using prism, graphpad).

Immunohistochemistry

For perfusion fixation, mice were given a lethal dose of ketamine (KETASET; Willows Francis, UK) and xylazine (ROMPUN, Bayer, Germany) and transcardially perfused with 50 mL phosphate-buffered saline (PBS; 0.1 m, pH 7.4) followed by 80 mL of 4% (w/v) paraformaldehyde (PFA; Sigma, UK) solution in PBS. Brains were removed and post-fixed for 1–5 h at 4 °C, in 4% PFA, then cryoprotected for 24 h at 4 °C, in 30% sucrose in PBS. They were subsequently embedded in OCT medium, frozen in isopentane at −50 °C and sectioned at 30 μm on a cryostat (Leica CM1800; Leica Microsystems). For single-cell labelling in brain slices, neurons were filled with neurobiotin (0.1%) and slices were incubated at 4 °C, in 4% (w/v PFA), in PBS overnight (or 45 min at room temperature).

For immunohistochemistry, fixed free-floating sections were subsequently washed in PBS containing 0.2% Triton X-100 (PBS-T 0.2%), and blocked in PBS-T 0.2% with 6% NDS (normal donkey serum; Jackson ImmunoResearch, USA) for 30 min at room temperature, and incubated overnight at room temperature in PBS-T 0.2% containing 2% NDS and primary antibodies: anti-serotonin (5HT) polyclonal rabbit antibody (1: 1000; Immunostar, USA); anti-TH monoclonal chicken antibody (1: 1000; Abcam, USA); anti-AADC (amino acid decarboxylase) rabbit antibody (1: 1000; Millipore, USA); and anti-VIP (vasoactive intestinal polypeptide) rabbit antibody (1: 500; Immunostar, USA). Sections were then rinsed in PBS-T 0.2% and incubated for 90 min at room temperature in PBS-T 0.2% containing 2% NDS and appropriate secondary antibodies: Cy3-conjugated anti-rabbit (1: 1000; Jackson ImmunoResearch); and Alexa 633-conjugated anti-chicken (1: 1000; Invitrogen, USA). AMCA-conjugated streptavidin (1: 1000; Jackson ImmunoResearch) was used to reveal neurobiotin labelling. Sections were finally rinsed three times in PBS-T 0.2%, twice in PBS and then mounted onto glass microscope slides in VectaShield (Vector Laboratories, USA) for confocal microscopy, and pictures were captured using CONFOCAL

Software (Leica Microsystems). Confocal laser scanning microscopy was performed using a Leica SP5 II confocal microscope through a 20 ×/0.7 numerical aperture dry HC Plan-Apochromat CS DIC objective, with 1.5 × digital zoom applied during image capture (30 × total magnification). GFP was excited by a 488-nm line of an Ar laser, Cy3 by a 561-nm line of a DPSS laser, AlexaFluor633 by a 633-nm line of an He–Ne laser, and AMCA by a 405-nm line of a diode laser. Images were taken at a resolution of 2048 × 2048 and were processed with general brightness and contrast curve adjustments in Adobe Photoshop CS5 (Adobe Systems Incorporated). Cell counts were based on totals from nine sections in each case for perfusion-fixed sections (i.e. three sections per animal, from three animals) and six brain slices in each case for post-fixed brain slices (i.e. one section per animal from six animals).

Results

Pitx3-GFP and TH-GFP expression in DRN/vlPAG

To conduct targeted recordings from DRN/vlPAG dopamine neurons we used two mouse models, Pitx3-GFP and TH-GFP mice. In Pitx3-GFP mice, GFP is inserted into the Pitx3 locus, resulting in Pitx3-directed GFP expression which almost completely overlaps with TH expression in the VTA and substantia nigra (Zhao *et al.*, 2004), and the GFP signal is strong enough to be used in brain slices to locate and record from dopamine neurons (e.g. Labouebe *et al.*, 2007). In TH-GFP mice, GFP is under the control of the TH promoter (Matsushita *et al.*, 2002). In these mice around 80% of VTA TH+ neurons are GFP+ (Matsushita *et al.*, 2002). Consistent with previous studies, we observed two types of TH+ neurons in the DRN/vlPAG: small, round/oval neurons, typically located close to the aqueduct; and larger, multipolar neurons located more ventrally (e.g. Hokfelt *et al.*, 1984b; Hasue & Shammah-Lagnado, 2002; Flores *et al.*, 2004; Meloni *et al.*, 2006). In both mouse models, we observed similar patterns of GFP and TH, although in Pitx3-GFP mice GFP expression was particularly strong in periaqueductal neurons compared with larger, more ventral neurons, whereas in the TH-GFP mice GFP expression was more uniform. In both cases most GFP+ neurons were TH+ (TH-GFP: 74%, 606/823 cells; Pitx3-GFP: 71%, 274/386 cells; Fig. 1A). GFP+/TH− neurons were typically small periaqueductal neurons. Because the GFP signal in the TH-GFP mice was under the control of the TH promoter, it seems likely that the small, periaqueductal GFP+/TH− neurons were dopaminergic. Moreover, most of these neurons were AADC+ (an essential enzyme for dopamine synthesis; TH-GFP: 72%, 510/704 cells), suggesting that they are dopaminergic but perhaps express TH at low levels (Fig. 1B; note that 5HT neurons are also AADC+ and therefore probably represent the AADC+/GFP) neurons seen in Fig. 1C). We observed that there was no overlap between GFP and 5HT (Fig. 1D). In addition, we observed some TH+ neurons that were GFP− (or GFP was below our detection threshold) (TH-GFP: 10%, 70/676 cells; Pitx3-GFP: 40% 183/457 cells), which were generally larger and located more ventrally.

The distributions of immunolabelling for TH and 5HT in the VTA and DRN that we observed were identical to previous reports. Moreover, we observed no immunolabelling if either primary or secondary antibodies were omitted. Although co-localization of TH and GFP was not complete (which is common generally in GFP mouse models, and indeed also

the case in the VTA of TH-GFP mice), these results suggest that these mouse lines can be used to help locate dopamine neurons in the DRN/vlPAG in acute brain slices for electrophysiological recordings and *post-hoc* anatomical and immunohistochemical analyses.

Co-expression of VIP

We also noted that the expression pattern of GFP close to the aqueduct in the DRN/vlPAG of Pitx3-GFP and TH-GFP mice was strikingly similar to that reported for the neuropeptide transmitter VIP (e.g. Fu *et al.*, 2010). We therefore wanted to see if VIP co-localized with GFP. VIP immunolabelling was identical to previous reports (Fu *et al.*, 2010; Fig. 2A), was absent in the VTA, and no labelling was observed if either the primary or the secondary antibody was omitted. All VIP+ neurons were also GFP+. Just over half of GFP+ neurons were VIP+, and these were typically located more dorsally (TH-GFP: 40%, 330/823 cells; Pitx3-GFP: 58%, 224/386 cells; Fig. 2A). Of these GFP+ VIP+ neurons, most were also TH + (TH-GFP: 75%, 246/330 cells; Pitx3-GFP: 76%, 171/224 cells).

Single-cell labelling in brain slices, AP properties and responses to depolarization and hyperpolarization

We prepared acute coronal brain slices from mice and conducted whole-cell recordings from single GFP+ neurons. Recording electrodes were filled with neurobiotin which diffused into the neuron during recording. Of the 160 GFP+ neurons that were successfully filled with neurobiotin and recovered for immunofluorescence, 84.5% of the Pitx3-GFP were TH+ (82/97 neurons) and 87.3% of the TH-GFP were TH+ (55/63 neurons), indicating that GFP+ neurons were TH+ in similar proportions in both mouse models ($\chi^2 = 0.24$, $P = 0.63$). These proportions were higher than what might be expected based on the degree of co-localization in perfusion-fixed sections, and may be related to brainslicing (rather than recording), as we observed a similarly high degree of co-localization when we examined non-recorded cells in post-fixed brain slices (TH-GFP: 83%, 403/485 cells; Pitx3-GFP: 76%, 247/325 cells). This could be because either the GFP+/TH− neurons are less likely to survive brainslicing, or their low levels of TH (undetectable in perfusion-fixed sections) are at detection level in brain slices. Regardless, these results show that GFP can be used as an effective means to target dopamine neurons in the DRN/vlPAG, the identity of which can be further confirmed using immunofluorescence.

Of those neurobiotin-filled TH+ neurons examined for VIP immunolabelling, a higher proportion were VIP+ in Pitx3-GFP mice (52%, 25/48 neurons) compared with TH-GFP mice (28%, 26/93 neurons; $\chi^2 = 5.86$, $P = 0.016$). These results are consistent with our observations that Pitx3-GFP signal was strongest in more dorsal neurons closer to the aqueduct, which are more likely to be VIP+. Interestingly, we observed increased co-localization of VIP and TH in post-fixed brain slices (similar to that seen for GFP and TH described above; TH-GFP: 87%, 248/286 cells; Pitx3-GFP: 88%, 203/231 cells). Together, these results show that these two different mouse models can be used to target both VIP+ and VIP− dopamine neurons within the DRN/vlPAG (with increased proportions of VIP− neurons in the TH-GFP case).

When recorded in current-clamp mode, most GFP+ neurons fired spontaneous APs (76% Pitx3-GFP, n = 19/25 neurons; 70% TH-GFP, n = 27/35 neurons) at rates (4.1 ± 0.4 Hz) and patterns (0.5 ± 0.04 CV-ISI; Fig. 2B) moderately higher than those typically reported for the VTA (e.g. Johnson & North, 1992; Neuhoff *et al.*, 2002; Gale & Perkel, 2006; Margolis *et al.*, 2006b; Lammel *et al.*, 2008), and significantly faster and more irregular than spontaneously firing putative DRN 5HT neurons (p5HT; see Materials and methods) (n = 14/25 neurons were spontaneously active; 1.3 ± 0.3 Hz; 0.31 ± 0.03 CV-ISI; $P < 0.05$). Interestingly, firing in VIP+ neurons was more irregular than in VIP− neurons (VIP+ 0.67 ± 0.13 CV-ISI, VIP− 0.33 ± 0.07 CV-ISI, $t_{31} = 2.238$, $P = 0.033$) although they fired at similar rates (VIP+ 3.7 ± 0.8 Hz, VIP− 4.5 ± 0.65 Hz, $t_{31} = 0.8$, $P = 0.43$). We did not observe any differences between Pitx3-GFP and TH-GFP neurons, or between TH+ and TH− neurons, in terms of firing rate and pattern (see Table 1).

Spontaneously firing GFP+ neurons exhibited broad APs (4.2 ± 0.2;ms), with a relatively depolarized threshold (−26.0 ± 1.1 mV), followed by a prominent afterhyperpolarization (−51.0 ± 1.3 mV), with a relatively slow afterhyperpolarization recovery rate (0.13 ± 0.01 mV/ms) (Fig. 2B), similar to most VTA dopamine neurons (e.g. Margolis *et al.*, 2006b; Lammel *et al.*, 2008). We did not observe any differences in these properties between Pitx3-GFP and TH-GFP neurons, or between identified TH+ and TH− neurons, or between VIP+ and VIP− neurons and consequently data have been pooled for the above values (see Table 1).

In response to small depolarizing current injection, Pitx3-GFP neurons fired rapidly throughout the pulse. However, in response to larger depolarizations, neurons exhibited spike-frequency adaptation, often entering depolarization block (n = 16; Fig. 3A). Similar properties were observed in TH-GFP neurons that were identified as either VIP+ or VIP− (n = 10 and 13; Fig. 3B–D) for instantaneous (interaction between group and depolarizing pulse amplitude, $F_{8,180} = 0.16$, $P = 0.99$; main effect of group, $F_{2,180} = 0.68$, $P = 0.51$; main effect of pulse amplitude, $F_{4,180} = 12.2$, $P < 0.0001$) and steady-state firing frequencies (interaction between group and depolarizing pulse amplitude, $F_{8,180} = 0.45$, $P = 0.89$; main effect of group, $F_{2,180} = 1.72$, $P = 0.18$; main effect of pulse amplitude, $F_{4,180} = 16.4$, $P < 0.0001$). In contrast, p5HT neurons fired at low frequencies, exhibited spike-frequency adaptation in response to all depolarizing pulses and did not enter depolarization block (n = 5; Fig. 4E).

In response to hyperpolarizing pulses in current-clamp and voltage-clamp mode, most GFP+ neurons exhibited a prominent hyperpolarization-activated inward current (I_h; Fig. 4A and B), not seen in p5HT neurons (all GFP+ −16.8 ± 1.4 pA, p5HT 5.6 ± 1.3 pA; n = 118 and 25; $t_{141} = 7.2$, $P < 0.0001$). This was blocked with the I_h blocker ZD7228 (10 μm) (87 ± 5% reduction, n = 6). I_h is a feature commonly seen in VTA and substantia nigra pars compacta (SNC) dopamine neurons, with the exception of meso-cortical VTA dopamine neurons (Lammel *et al.*, 2008). It should be noted also that some non-dopamine neurons in the VTA exhibit an I_h (Margolis *et al.*, 2006b). Consistent with this, we found no differences in I_h between GFP+ neurons that were immunolabelled either TH+ and TH− (TH+ −35.1 ± 2.7 pA, TH− −36.4 ± 8.8 pA; n = 22 and 6; $t_{26} = 0.19$, $P = 0.84$). Interestingly, VIP− neurons typically exhibited relatively small I_h, whereas VIP+ neurons exhibited a broader range of I_h

values, from relatively small to large, that were on average larger compared with VIP− neurons (Fig. 4C; VIP+ −22.2 ± 5.2 pA, VIP− −6.9 ± 1.0 pA; n = 25 and 32; t_{55} = 5.14, P < 0.0001). Consistent with our observation that more TH-GFP neurons are VIP−, we observed smaller I_h on average in TH-GFP neurons compared with all Pitx3-GFP neurons (TH-GFP −12.1 ± 1.6 pA, Pitx3-GFP −20.1 ± 2.0 pA; n = 48 and 70; t_{116} = 2.9, P = 0.0047).

In addition, GFP+ neurons exhibited a large, outward residual current following the hyperpolarizing pulse (Fig. 4A and B), not seen in p5HT neurons (all GFP+ 202.0 ± 14.9 pA, p5HT −13.8 ± 7.2 pA; n = 118 and 25; t_{141} = 6.6, P < 0.0001). This mediates the delayed repolarization seen in current-clamp following hyperpolarization (Fig. 4A). This current was blocked by the A-current blocker 4-AP (5 mm) (94 ± 4% reduction, n = 6). We did not observe any differences between Pitx3-GFP and TH-GFP neurons (Pitx3-GFP 208.7 ± 20.1 pA, TH-GFP 192.2 ± 22.3 pA; n = 48 and 70; t_{116} = 0.54, P = 0.6) or between identified VIP+ and VIP− neurons (Fig. 4C; VIP+ 164.3 ± 25.1 pA, VIP− 172.9 ± 21.1 pA; n = 25 and 32; t_{55} = 0.266, P = 0.79).

Using these hyperpolarizing pulses in voltage clamp, we also measured input resistance, which was relatively high compared with p5HT neurons (all GFP+ 1.38 ± 0.12 GΩ, p5HT 0.58 ± 0.05 GΩ; n = 101 and 25; t_{124} = 3.39, P = 0.0009) and reported values for VTA and SNC dopamine neurons. In addition, these values did not differ between Pitx3-GFP and TH-GFP neurons (Pitx3-GFP 1.23 ± 0.11 GΩ, TH-GFP 1.64 ± 0.26 GΩ; n = 36 and 65; t_{99} = 1.7, P = 0.09), or between TH+ and TH− neurons (TH+ 1.75 ± 0.27 GΩ, TH− 1.02 ± 0.13 GΩ; n = 37 and 8; t_{43} = 1.26, P = 0.22), or between VIP+ and VIP− neurons (VIP+ 1.75 ± 0.4 GΩ, VIP− 1.52 ± 0.23 GΩ; n = 21 and 24; t_{43} = 0.49, P = 0.63). In addition, we did not observe any differences between Pitx3-GFP and TH-GFP (Pitx3-GFP 12.03 ± 0.97 pF, TH-GFP 12.0 ± 0.53 pF; n = 26 and 52; t_{76} = 0.23, P = 0.82), or between TH+ and TH− neurons (TH+ 12.4 ± 0.66 pF, TH− 12.5 ± 1.2 pF; n = 49 and 10; t_{57} = 0.045, P = 0.96) with respect to whole-cell capacitance, but VIP+ neurons had smaller whole-cell capacitance measurements compared with VIP−, consistent with their observed smaller size (VIP+ 9.6 ± 0.7 pF; VIP− 12.9 ± 1.2 pF; n = 27 and 33; t_{58} = 2.55, P = 0.014).

Synaptic physiology

Next we examined synaptic events in Pitx3-GFP and p5HT neurons. In all cases we were able to record sEPSCs of −70 mV that were abolished by NBQX (5 μm; n = 6), showing that they are AMPA receptor-mediated glutamatergic events. Pitx3-GFP neurons had lower frequency and lower amplitude sEPSCs compared with p5HT neurons (Freq: t_{19} = 2.85, P = 0.01; Amp: t_{19} = 6.38, P < 0.0001; n = 12 and 9; Fig. 5A and B). We also attempted to evoke synaptic events using a bipolar extracellular stimulating electrode. This was initially quite challenging, but after some practice became possible. It was particularly dependent on the positioning of the extracellular stimulating electrode, ideally around 100 μm ventro-lateral to the recorded neuron. Paired-pulse eEPSC ratios (PPRs) in Pitx3-GFP neurons tended towards depression (i.e. < 1.0) and facilitation (i.e. > 1.0) for p5HT neurons (t_{27} = 3.57, P = 0.0014; n = 19 and 10; Fig. 5C and D). We also evoked combined AMPAR- and NMDAR-mediated EPSCs at +40 mV. AP5 (the NMDAR antagonist) was subsequently applied to leave a pure AMPA component. This was subtracted from the combined

AMPAR/NMDAR EPSC to provide a computed NMDAR-only EPSC, and AMPAR/NMDAR ratios (of the peaks) were calculated. Pitx3-GFP neurons exhibited relatively high ratios, compared with those reported for VTA dopamine neurons (e.g. Ungless *et al.*, 2001; Lammel *et al.*, 2011), but these were significantly smaller than p5HT neurons ($t_{12} = 3.57$, $P = 0.016$; $n = 6$ and 8; Fig. 5E and F). Higher ratios than those seen in the VTA could be because there is a greater AMPAR-mediated component or a smaller NMDAR-mediated component, or both.

In addition, we also observed sIPSCs at 0 mV that were completely abolished by the $GABA_A$ receptor antagonist picrotoxin (100 μm, $n = 4$). We observed low frequencies of events in p5HT neurons, possibly related to their large size which increased noise at 0 mV precluding the detection of smaller events (Freq: $t_{19} = 3.79$, $P = 0.0013$; Amp: $t_{19} = 0.31$, $P = 0.76$; $n = 12$ and 9; Fig. 5G and H). However, in all groups it was possible to evoke IPSCs with a stimulating electrode at 0 mV. We observed paired-pulse facilitation in Pitx3-GFP and paired-pulse depression in p5HT neurons ($t_{27} = 2.06$, $P = 0.049$; $n = 19$ and 10; Fig. 5I and J).

Lastly, we conducted a comparison of synaptic physiology between identified VIP+ and VIP − neurons from TH-GFP mice. As for Pitx3-GFP neurons, in all cases we were able to record sEPSCs at −70 mV that were abolished by NBQX (5 μm; $n = 5$). VIP+ neurons had lower frequency and lower amplitude sEPSCs compared with VIP) neurons (Freq: $t_{24} = 2.62$, $P = 0.015$; Amp: $t_{24} = 2.73$, $P = 0.012$; $n = 9$ and 17; Fig. 6A and B). In addition, paired-pulse eEPSC ratios (PPRs) were lower in VIP+ neurons than in VIP− neurons ($t_{16} = 2.28$, $P = 0.037$; $n = 8$ and 10; Fig. 6C and D). AMPAR/NMDAR ratios were similar in VIP + and VIP− neurons ($t_{12} = 0.36$, $P = 0.73$; $n = 4$ and 10; Fig. 6E and F).

As for Pitx3-GFP neurons, we also observed sIPSCs at 0 mV that were completely abolished by the $GABA_A$ receptor antagonist picrotoxin (100 μm, $n = 5$). We observed low frequencies of events in VIP− neurons, possibly related to their larger size, compared with VIP+ neurons, which increased noise at 0 mV, precluding the detection of smaller events (Freq: $t_{20} = 2.0$, $P = 0.059$; Amp: $t_{20} = 1.13$, $P = 0.204$; $n = 9$ and 13; Fig. 6G and H). However, it was possible to evoke IPSCs with a stimulating electrode at 0 mV. We observed paired-pulse facilitation in both groups ($t_{13} = 0.068$, $P = 0.95$; $n = 6$ and 9; Fig. 6I and J). These results indicate that GABAergic synaptic transmission is similar in VIP+ and VIP− neurons.

Discussion

We have used two mouse models (Pitx3-GFP and TH-GFP) to conduct targeted whole-cell recordings from dopamine neurons in acute brain slices containing the DRN and vlPAG. Consistent with previous reports, we find two anatomically distinct groups of dopamine neurons: small, typically bipolar fusiform neurons mostly located in the periaqueductal region, and large, multipolar neurons scattered more ventrally. Interestingly, we have found that many small, periaqueductal DRN/vlPAG dopamine neurons also co-express the neuropeptide VIP. Presumably, these neurons are co-releasing VIP as a neuromodulator. Consistent with this, VIP projections from this region overlap with dopaminergic

projections, particularly in the dorso-lateral bed nucleus of the stria terminalis (dlBNST; Eiden *et al.*, 1985; Petit *et al.*, 1995; Kozicz *et al.*, 1998; Hasue & Shammah-Lagnado, 2002) where they synapse onto corticotrophin-releasing factor neurons (Kozicz *et al.*, 1997). Little is known about the function of VIP in this region, although in the hypothalamus it appears to play a role in regulating circadian rhythms (Aton *et al.*, 2005). Interestingly, VIP receptor 2 duplications have been associated with risk for schizophrenia (Vacic *et al.*, 2011), which has been traditionally viewed as a dopaminergic disorder. This adds to a list of neuropeptides co-expressed by subgroups of midbrain dopamine neurons, including cholecystokinin and neurotensin (Hokfelt *et al.*, 1984a; Seroogy *et al.*, 1988, 1989). It is not clear, however, why only certain subgroups co-release neuropeptides.

The dopamine neurons of the DRN/vlPAG described here exhibited electrophysiological properties very similar to VTA dopamine neurons, but distinct from neighbouring 5HT DRN neurons. In addition, we did not observe any major differences between TH-GFP and Pitx3-GFP neurons, suggesting that those particular genetic manipulations do not affect basic electrophysiological properties of the cells. They have, for example, slow firing rates, broad APs with prominent afterhyperpolarizations and a hyperpolarization-activated inward current. They also exhibit pronounced spike-frequency adaptation, and often entered depolarization block in response to strong depolarizations. In addition, they exhibit a distinct delayed repolarization following hyperpolarization. It may be, therefore, that these properties could be used to identify dopamine neurons in the DRN/vlPAG based on electrophysiological properties alone.

We did not observe major differences in these properties between VIP+ and VIP− dopamine neurons. One notable exception was the hyperpolarization-activated inward current (I_h), which was prominent in VIP+ neurons, but small or absent in most VIP− neurons. In the VTA, I_h is commonly used as a predictor of dopaminergic identity, but dopaminergic neurons in more medial regions, particularly projecting to prefrontal cortex, amygdala and accumbens core, appear to lack a prominent I_h current (Lammel *et al.*, 2008; but see Margolis *et al.*, 2006a). It is therefore tempting to speculate that in the DRN I_h may also distinguish between different projection systems. Indeed, the VIP projection from the DRN/vlPAG appears to be relatively restricted, innervating only the dlBNST (Eiden *et al.*, 1985; Petit *et al.*, 1995; Kozicz *et al.*, 1998). In contrast, dopaminergic projections from the DRN/vlPAG innervate multiple regions including the lateral hypothalamus, latero-dorsal tegmentum and locus coeruleus (Lu *et al.*, 2006).

We also recorded fast glutamatergic and GABAergic synaptic transmission in DRN/vlPAG dopamine neurons. These neurons receive excitatory inputs from a number of regions, including a glutamatergic projection from the prefrontal cortex (Lu *et al.*, 2006). One notable source of inhibitory, GABAergic input comes from the sleep-promoting ventrolateral preoptic nucleus region in the hypothalamus (Lu *et al.*, 2006). Although evoking synaptic events in these neurons (in coronal slices) was not as straightforward as in the VTA (in horizontal slices; it is more challenging to evoke synaptic currents in the VTA in coronal slices), this initial characterization will pave the way for future studies. Given their distinct role in promoting wakefulness, it will be interesting to see if they exhibit cocaine- and ethanol-induced synaptic plasticity as seen in the VTA (Ungless *et al.*, 2001;

Melis *et al.*, 2002), especially in light of recent reports that VTA dopamine neurons exhibit different types of stress- and cocaine-induced plasticity depending on their projection targets (Lammel *et al.*, 2011).

An important step towards understanding the functional role of these neurons will be to examine their electrophysiological properties *in vivo* in awake animals. c-Fos studies suggest that they may change their activity across the sleep–wake cycle (Lu *et al.*, 2006; but see Leger *et al.*, 2010). Indeed, it is possible that previous studies that have reported changes in DRN neurons across sleep–wake periods may in some cases have sampled these dopamine neurons (e.g. Urbain *et al.*, 2006). However, single-cell labelling studies in anaesthetized rats suggest that spontaneously active dopamine neurons are rarely encountered with an extracellular electrode: although several studies have sampled widely in the DRN (e.g. Allers & Sharp, 2003), only one dopamine neuron has been successfully labelled and identified with immunolabelling (Schweimer & Ungless, 2010). This suggests that, in the absence of unique electrophysiological identifiers *in vivo*, other approaches will be required to examine this population. One possibility may be to use optogenetics to selectively express channelrhodopsin in dopamine neurons in the DRN (as has been done successfully in the VTA; Tsai *et al.*, 2009). This would allow for the identification of and recording from dopamine neurons using a combined light probe and electrode, and also potentially for the direct and selective manipulation of their activity to investigate their role in modulating behaviour.

Acknowledgements

This research was supported by grant U120085816 from the UK Medical Research Council (MRC) and a University Research Fellowship from The Royal Society to M.A.U.

Abbreviations

AADC	amino acid decarboxylase
aCSF	artificial cerebrospinal fluid
AHP	afterhyperpolarisation
AMPAR	α-amino-3-hydroxy-5-methyl-4-isoxazole-propionic acid receptor
AP	action potential
CV-ISI	coefficient of variation of the inter-spike-interval
dlBNST	dorso-lateral bed nucleus of the stria terminalis
DRN	dorsal raphe nucleus
IR-DIC	infra-red differential interference contrast
NDS	normal donkey serum
NMDAR	*N*-methyl-D-aspartate receptor
PBS	phosphate-buffered saline

PPR	paired-pulse ratio
sEPSCs	excitatory post-synaptic currents
sIPSCs	inhibitory post-synaptic currents
SNC	substantia nigra pars compacta
TH	tyrosine hydroxylase
VIP	vasoactive intestinal polypeptide
vlPAG	ventrolateral periaqueductal grey
VTA	ventral tegmental area

References

Allers KA, Sharp T. Neurochemical and anatomical identification of fast- and slow-firing neurones in the rat dorsal raphe nucleus using juxtacellular labelling methods in vivo. Neuroscience. 2003; 122:193–204. [PubMed: 14596860]

Arsenault MY, Parent A, Seguela P, Descarries L. Distribution and morphological characteristics of dopamine-immunoreactive neurons in the midbrain of the squirrel monkey (Saimiri sciureus). J. Comp. Neurol. 1988; 267:489–506. [PubMed: 3346372]

Aton SJ, Colwell CS, Harmar AJ, Waschek J, Herzog ED. Vasoactive intestinal polypeptide mediates circadian rhythmicity and synchrony in mammalian clock neurons. Nat. Neurosci. 2005; 8:476–483. [PubMed: 15750589]

Beck SG, Pan YZ, Akanwa AC, Kirby LG. Median and dorsal raphe neurons are not electrophysiologically identical. J. Neurophysiol. 2004; 91:994–1005. [PubMed: 14573555]

Charara A, Parent A. Chemoarchitecture of the primate dorsal raphe nucleus. J. Chem. Neuroanat. 1998; 15:111–127. [PubMed: 9719363]

Dahan L, Astier B, Vautrelle N, Urbain N, Kocsis B, Chouvet G. Prominent burst firing of dopaminergic neurons in the ventral tegmental area during paradoxical sleep. Neuropsychopharmacol. 2007; 32:1232–1241.

Descarries L, Berthelet F, Garcia S, Beaudet A. Dopaminergic projection from nucleus raphe dorsalis to neostriatum in the rat. J. Comp. Neurol. 1986; 249:511–520. [PubMed: 2427554]

Edwards FA, Konnerth A, Sakmann B, Takahashi T. A thin slice preparation for patch clamp recordings from neurones of the mammalian central nervous system. Pflugers Arch. 1989; 414:600–612. [PubMed: 2780225]

Eiden LE, Hokfelt T, Brownstein MJ, Palkovits M. Vasoactive intestinal polypeptide afferents to the bed nucleus of the stria terminalis in the rat: an immunohistochemical and biochemical study. Neuroscience. 1985; 15:999–1013. [PubMed: 3900807]

Flores JA, El Banoua F, Galan-Rodriguez B, Fernandez-Espejo E. Opiate anti-nociception is attenuated following lesion of large dopamine neurons of the periaqueductal grey: critical role for D1 (not D2) dopamine receptors. Pain. 2004; 110:205–214. [PubMed: 15275769]

Flores JA, Galan-Rodriguez B, Ramiro-Fuentes S, Fernandez-Espejo E. Role for dopamine neurons of the rostral linear nucleus and periaqueductal gray in the rewarding and sensitizing properties of heroin. Neuropsychopharmacol. 2006; 31:1475–1488.

Fu W, Le Maitre E, Fabre V, Bernard JF, David Xu ZQ, Hokfelt T. Chemical neuroanatomy of the dorsal raphe nucleus and adjacent structures of the mouse brain. J. Comp. Neurol. 2010; 518:3464–3494. [PubMed: 20589909]

Gale SD, Perkel DJ. Physiological properties of zebra finch ventral tegmental area and substantia nigra pars compacta neurons. J. Neurophysiol. 2006; 96:2295–2306. [PubMed: 16870835]

Hara J, Beuckmann CT, Nambu T, Willie JT, Chemelli RM, Sinton CM, Sugiyama F, Yagami K, Goto K, Yanagisawa M, Sakurai T. Genetic ablation of orexin neurons in mice results in narcolepsy, hypophagia, and obesity. Neuron. 2001; 30:345–354. [PubMed: 11394998]

Hasue RH, Shammah-Lagnado SJ. Origin of the dopaminergic innervation of the central extended amygdala and accumbens shell: a combined retrograde tracing and immunohistochemical study in the rat. J. Comp. Neurol. 2002; 454:15–33. [PubMed: 12410615]

Hokfelt T, Everitt BJ, Theodorsson-Norheim E, Goldstein M. Occurrence of neurotensinlike immunoreactivity in subpopulations of hypothalamic, mesencephalic, and medullary catecholamine neurons. J. Comp. Neurol. 1984a; 222:543–559. [PubMed: 6365985]

Hokfelt, T.; Martensson, R.; Bjorklund, A.; Kleinau, S.; Goldstein, M. Distribution of tyrosine-hydroxylase-immunoreactive neurons in the rat brain. In: Bjorklund, A.; Hokfelt, T., editors. Handbook of Chemical Neuroanatomy. Elsevier Science; Amsterdam: 1984b. p. 277-379.

Johnson SW, North RA. Two types of neurone in the rat ventral tegmental area and their synaptic inputs. J. Physiol. 1992; 450:455–468. [PubMed: 1331427]

Kozicz T, Vigh S, Arimura A. Axon terminals containing PACAP- and VIP-immunoreactivity form synapses with CRF-immunoreactive neurons in the dorsolateral division of the bed nucleus of the stria terminalis in the rat. Brain Res. 1997; 767:109–119. [PubMed: 9365022]

Kozicz T, Vigh S, Arimura A. The source of origin of PACAP- and VIP-immunoreactive fibers in the laterodorsal division of the bed nucleus of the stria terminalis in the rat. Brain Res. 1998; 810:211–219. [PubMed: 9813333]

Krout KE, Jansen AS, Loewy AD. Periaqueductal gray matter projection to the parabrachial nucleus in rat. J. Comp. Neurol. 1998; 401:437–454. [PubMed: 9826272]

Labouebe G, Lomazzi M, Cruz HG, Creton C, Lujan R, Li M, Yanagawa Y, Obata K, Watanabe M, Wickman K, Boyer SB, Slesinger PA, Luscher C. RGS2 modulates coupling between GABAB receptors and GIRK channels in dopamine neurons of the ventral tegmental area. Nat. Neurosci. 2007; 10:1559–1568. [PubMed: 17965710]

Lai YY, Shalita T, Hajnik T, Wu JP, Kuo JS, Chia LG, Siegel JM. Neurotoxic N-methyl-D-aspartate lesion of the ventral midbrain and meso-pontine junction alters sleep-wake organization. Neuroscience. 1999; 90:469–483. [PubMed: 10215152]

Lammel S, Hetzel A, Hackel O, Jones I, Liss B, Roeper J. Unique properties of mesoprefrontal neurons within a dual mesocorticolimbic dopamine system. Neuron. 2008; 57:760–773. [PubMed: 18341995]

Lammel S, Ion DI, Roeper J, Malenka RC. Projection-specific modulation of dopamine neuron synapses by aversive and rewarding stimuli. Neuron. 2011; 70:855–862. [PubMed: 21658580]

Leger L, Sapin E, Goutagny R, Peyron C, Salvert D, Fort P, Luppi PH. Dopaminergic neurons expressing Fos during waking and paradoxical sleep in the rat. J. Chem. Neuroanat. 2010; 39:262–271. [PubMed: 20211244]

Lu J, Jhou TC, Saper CB. Identification of wake-active dopaminergic neurons in the ventral periaqueductal gray matter. J. Neurosci. 2006; 26:193–202. [PubMed: 16399687]

Luo AH, Aston-Jones G. Circuit projection from suprachiasmatic nucleus to ventral tegmental area: a novel circadian output pathway. Eur. J. Neurosci. 2009; 29:748–760. [PubMed: 19200068]

Luo AH, Georges FE, Aston-Jones GS. Novel neurons in ventral tegmental area fire selectively during the active phase of the diurnal cycle. Eur. J. Neurosci. 2008; 27:408–422. [PubMed: 18215237]

Luscher C, Ungless MA. The mechanistic classification of addictive drugs. PLoS Med. 2006; 3:e437. [PubMed: 17105338]

Maloney KJ, Mainville L, Jones BE. c-Fos expression in dopaminergic and GABAergic neurons of the ventral mesencephalic tegmentum after paradoxical sleep deprivation and recovery. Eur. J. Neurosci. 2002; 15:774–778. [PubMed: 11886456]

Margolis EB, Lock H, Chefer VI, Shippenberg TS, Hjelmstad GO, Fields HL. Kappa opioids selectively control dopaminergic neurons projecting to the prefrontal cortex. Proc. Natl. Acad. Sci. USA. 2006a; 103:2938–2942. [PubMed: 16477003]

Margolis EB, Lock H, Hjelmstad GO, Fields HL. The ventral tegmental area revisited: is there an electrophysiological marker for dopaminergic neurons? J. Physiol. 2006b; 577:907–924. [PubMed: 16959856]

Matsushita N, Okada H, Yasoshima Y, Takahashi K, Kiuchi K, Kobayashi K. Dynamics of tyrosine hydroxylase promoter activity during midbrain dopaminergic neuron development. J. Neurochem. 2002; 82:295–304. [PubMed: 12124430]

Melis M, Camarini R, Ungless MA, Bonci A. Long-lasting potentiation of GABAergic synapses in dopamine neurons after a single in vivo ethanol exposure. J. Neurosci. 2002; 22:2074–2082. [PubMed: 11896147]

Meloni EG, Gerety LP, Knoll AT, Cohen BM, Carlezon WA Jr. Behavioral and anatomical interactions between dopamine and corticotropin-releasing factor in the rat. J. Neurosci. 2006; 26:3855–3863. [PubMed: 16597740]

Meyer PJ, Morgan MM, Kozell LB, Ingram SL. Contribution of dopamine receptors to periaqueductal gray-mediated antinociception. Psychopharmacology. 2009; 204:531–540. [PubMed: 19225762]

Miller JD, Farber J, Gatz P, Roffwarg H, German DC. Activity of mesencephalic dopamine and non-dopamine neurons across stages of sleep and walking in the rat. Brain Res. 1983; 273:133–141. [PubMed: 6616218]

Neuhoff H, Neu A, Liss B, Roeper J. I(h) channels contribute to the different functional properties of identified dopaminergic subpopulations in the midbrain. J. Neurosci. 2002; 22:1290–1302. [PubMed: 11850457]

Petit JM, Luppi PH, Peyron C, Rampon C, Jouvet M. VIP-like immunoreactive projections from the dorsal raphe and caudal linear raphe nuclei to the bed nucleus of the stria terminalis demonstrated by a double immunohistochemical method in the rat. Neurosci. Lett. 1995; 193:77–80. [PubMed: 7478163]

Sawamoto K, Nakao N, Kobayashi K, Matsushita N, Takahashi H, Kakishita K, Yamamoto A, Yoshizaki T, Terashima T, Murakami F, Itakura T, Okano H. Visualization, direct isolation, and transplantation of midbrain dopaminergic neurons. Proc. Natl. Acad. Sci. USA. 2001; 98:6423–6428. [PubMed: 11353855]

Schultz W. Getting formal with dopamine and reward. Neuron. 2002; 36:241–263. [PubMed: 12383780]

Schweimer JV, Ungless MA. Phasic responses in dorsal raphe serotonin neurons to noxious stimuli. Neuroscience. 2010; 171:1209–1215. [PubMed: 20888395]

Seroogy K, Ceccatelli S, Schalling M, Hokfelt T, Frey P, Walsh J, Dockray G, Brown J, Buchan A, Goldstein M. A subpopulation of dopaminergic neurons in rat ventral mesencephalon contains both neurotensin and cholecystokinin. Brain Res. 1988; 455:88–98. [PubMed: 3046712]

Seroogy KB, Dangaran K, Lim S, Haycock JW, Fallon JH. Ventral mesencephalic neurons containing both cholecystokinin- and tyrosine hydroxylase-like immunoreactivities project to forebrain regions. J. Comp. Neurol. 1989; 279:397–414. [PubMed: 2563737]

Stratford TR, Wirtshafter D. Ascending dopaminergic projections from the dorsal raphe nucleus in the rat. Brain Res. 1990; 511:173–176. [PubMed: 1970510]

Takada M, Campbell KJ, Moriizumi T, Hattori T. On the origin of the dopaminergic innervation of the paraventricular thalamic nucleus. Neurosci. Lett. 1990; 115:33–36. [PubMed: 1699175]

Trulson ME, Cannon MS, Raese JD. Identification of dopamine-containing cell bodies in the dorsal and median raphe nuclei of the rat brain using tyrosine hydroxylase immunochemistry. Brain Res. Bull. 1985; 15:229–234. [PubMed: 2864116]

Tsai HC, Zhang F, Adamantidis A, Stuber GD, Bonci A, de Lecea L, Deisseroth K. Phasic firing in dopaminergic neurons is sufficient for behavioral conditioning. Science. 2009; 324:1080–1084. [PubMed: 19389999]

Ungless MA, Whistler JL, Malenka RC, Bonci A. Single cocaine exposure in vivo induces long-term potentiation in dopamine neurons. Nature. 2001; 411:583–587. [PubMed: 11385572]

Urbain N, Creamer K, Debonnel G. Electrophysiological diversity of the dorsal raphe cells across the sleep-wake cycle of the rat. J. Physiol. 2006; 573:679–695. [PubMed: 16613874]

Vacic V, McCarthy S, Malhotra D, Murray F, Chou HH, Peoples A, Makarov V, Yoon S, Bhandari A, Corominas R, Iakoucheva LM, Krastoshevsky O, Krause V, Larach-Walters V, Welsh DK, Craig D, Kelsoe JR, Gershon ES, Leal SM, Dell Aquila M, Morris DW, Gill M, Corvin A, Insel PA, McClellan J, King MC, Karayiorgou M, Levy DL, DeLisi LE, Sebat J. Duplications of the

neuropeptide receptor gene VIPR2 confer significant risk for schizophrenia. Nature. 2011; 471:499–503. [PubMed: 21346763]

Wenk GL, Stoehr JD, Quintana G, Mobley S, Wiley RG. Behavioral, biochemical, histological, and electrophysiological effects of 192 IgG-saporin injections into the basal forebrain of rats. J. Neurosci. 1994; 14:5986–5995. [PubMed: 7523630]

Wise RA. Dopamine, learning and motivation. Nat. Rev. Neurosci. 2004; 5:483–494. [PubMed: 15152198]

Yoshida M, Shirouzu M, Tanaka M, Semba K, Fibiger HC. Dopaminergic neurons in the nucleus raphe dorsalis innervate the prefrontal cortex in the rat: a combined retrograde tracing and immunohistochemical study using anti-dopamine serum. Brain Res. 1989; 496:373–376. [PubMed: 2804651]

Zhao S, Maxwell S, Jimenez-Beristain A, Vives J, Kuehner E, Zhao J, O'Brien C, de Felipe C, Semina E, Li M. Generation of embryonic stem cells and transgenic mice expressing green fluorescence protein in midbrain dopaminergic neurons. Eur. J. Neurosci. 2004; 19:1133–1140. [PubMed: 15016072]

Europe PMC Funders Author Manuscripts

Europe PMC Funders Author Manuscripts

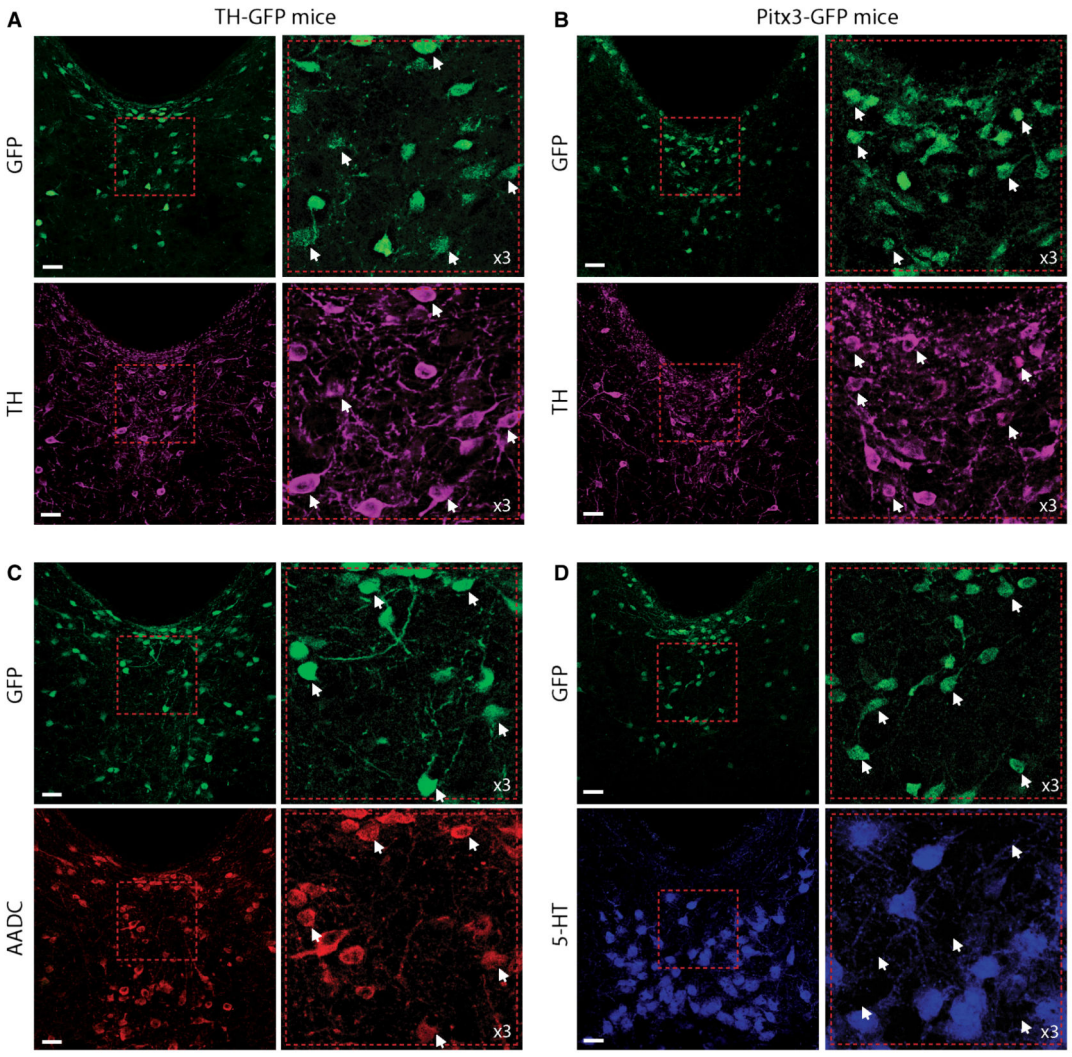

Fig. 1.

Distribution of GFP+ neurons, and co-localization with tyrosine hydroxylase (TH) in the dorsal raphe nucleus/ventro-lateral periaqueductal grey (DRN/vlPAG) in perfusion-fixed sections from Pitx3-GFP and TH-GFP mice. (A) Examples of GFP and TH distribution and co-localization in the DRN/vlPAG from TH-GFP mice (example neurons indicated by white arrows). (B) Examples of GFP and TH distribution and co-localization in the DRN/vlPAG from Pitx3-GFP mice (example neurons indicated by white arrows). (C) Example of GFP+ and AADC+ neuron distribution in the DRN/vlPAG, showing GFP+ neurons are also AADC+ (example neurons indicated by white arrows) (large ventral AADC+/GFP− neurons are 5HT neurons). (D) Example of GFP+ and 5HT+ neuron distribution in the DRN/vlPAG, showing no co-localization (example neurons indicated by white arrows). Scale bars = 30 μm.

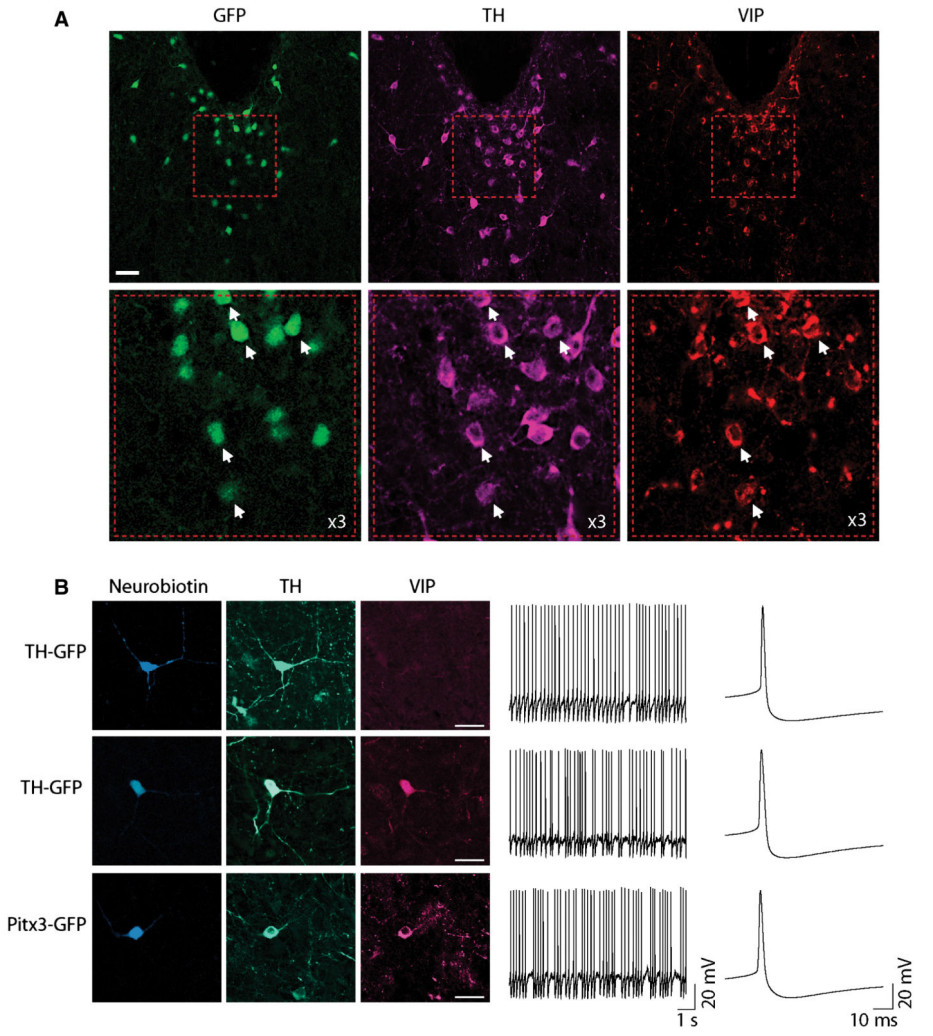

Fig. 2.

Vaso-active intestinal polypeptide (VIP) co-localization and firing properties of neurochemically identified DRN/vlPAG dopamine neurons. (A) Example of GFP, TH and VIP expression in DRN/vlPAG. VIP is more strongly expressed in periaqueductal GFP+ neurons (example triple immunopositive neurons indicated by white arrows). Scale bars = 30 μm. (B) Examples of neurobiotin-filled GFP+, TH+ neurons that are either VIP+ or VIP −. Scale bars = 30 μm. Firing rate and pattern and action potential properties are similar in both TH-GFP and Pitx3-GFP mice, and between VIP+ and VIP− dopamine neurons.

Europe PMC Funders Author Manuscripts

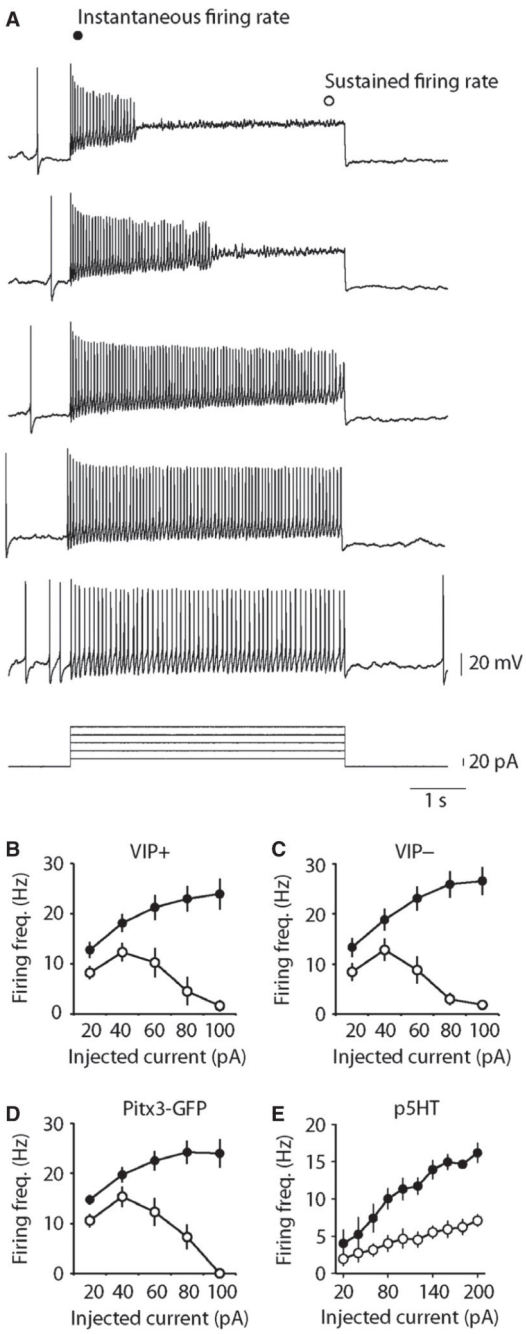

Fig. 3.

DRN/vlPAG dopamine neurons exhibit depolarization-induced spike-frequency adaptation. (A) Example of the effects of depolarizing pulses on AP firing in an identified Pitx3-GFP dopamine neuron. Graphs showing group average responses to depolarizing pulses in TH-GFP/VIP+ (*n* = 10) (B), TH-GFP/VIP− (*n* = 13) (C), Pitx3-GFP+ (not labelled with neurobiotin, *n* = 16) (D) and putative 5HT (GFP−, *n* = 5) neurons (E). All three groups of GFP+ neurons exhibit clear depolarization-induced spike-frequency adaptation often leading

to depolarization block. In contrast, p5HT neurons exhibit strong spike-frequency adaptation with increasing depolarization, but do not enter depolarization block.

Europe PMC Funders Author Manuscripts

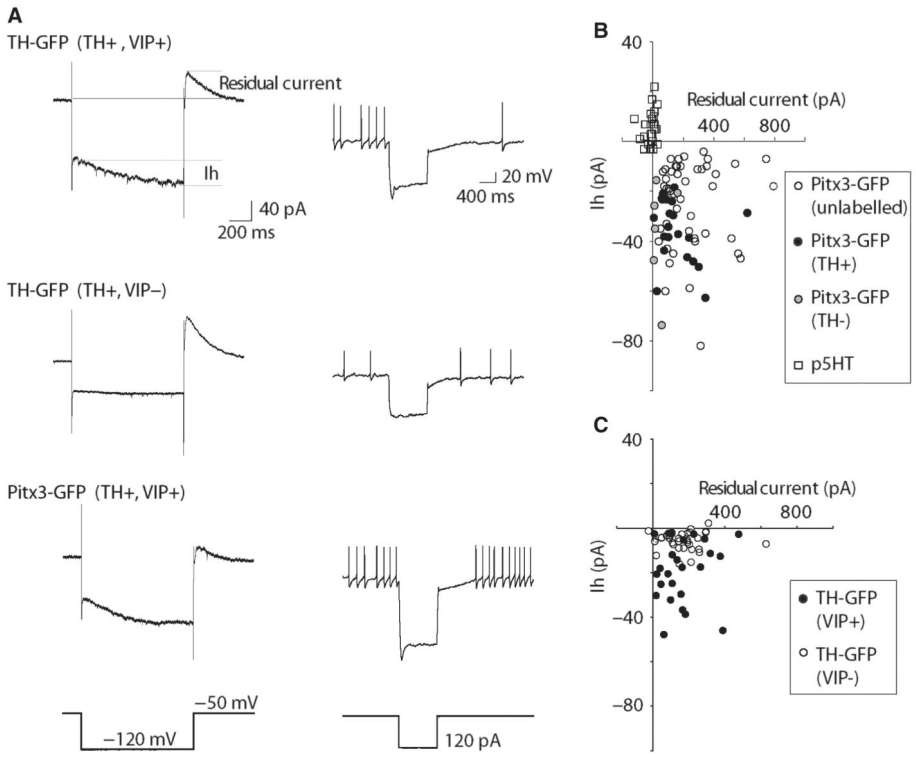

Fig. 4.

DRN/vlPAG dopamine neurons exhibit a hyperpolarization-activated inward current (I_h), which is largest in the VIP+ subgroup. Both groups exhibit an outward residual current following the hyperpolarization that probably contributes to delayed repolarization seen in current clamp. (A) Examples of voltage-clamp (left-hand traces) and current-clamp (right-hand traces) responses to hyperpolarization in different GFP+ neurons. (B) Scatter plot showing I_h and residual current values for Pitx3-GFP+ neurons and p5HT neurons. (C) Scatter plot showing I_h and residual current values for TH-GFP+ neurons neurochemically identified as dopaminergic and either VIP+ or VIP−.

Europe PMC Funders Author Manuscripts

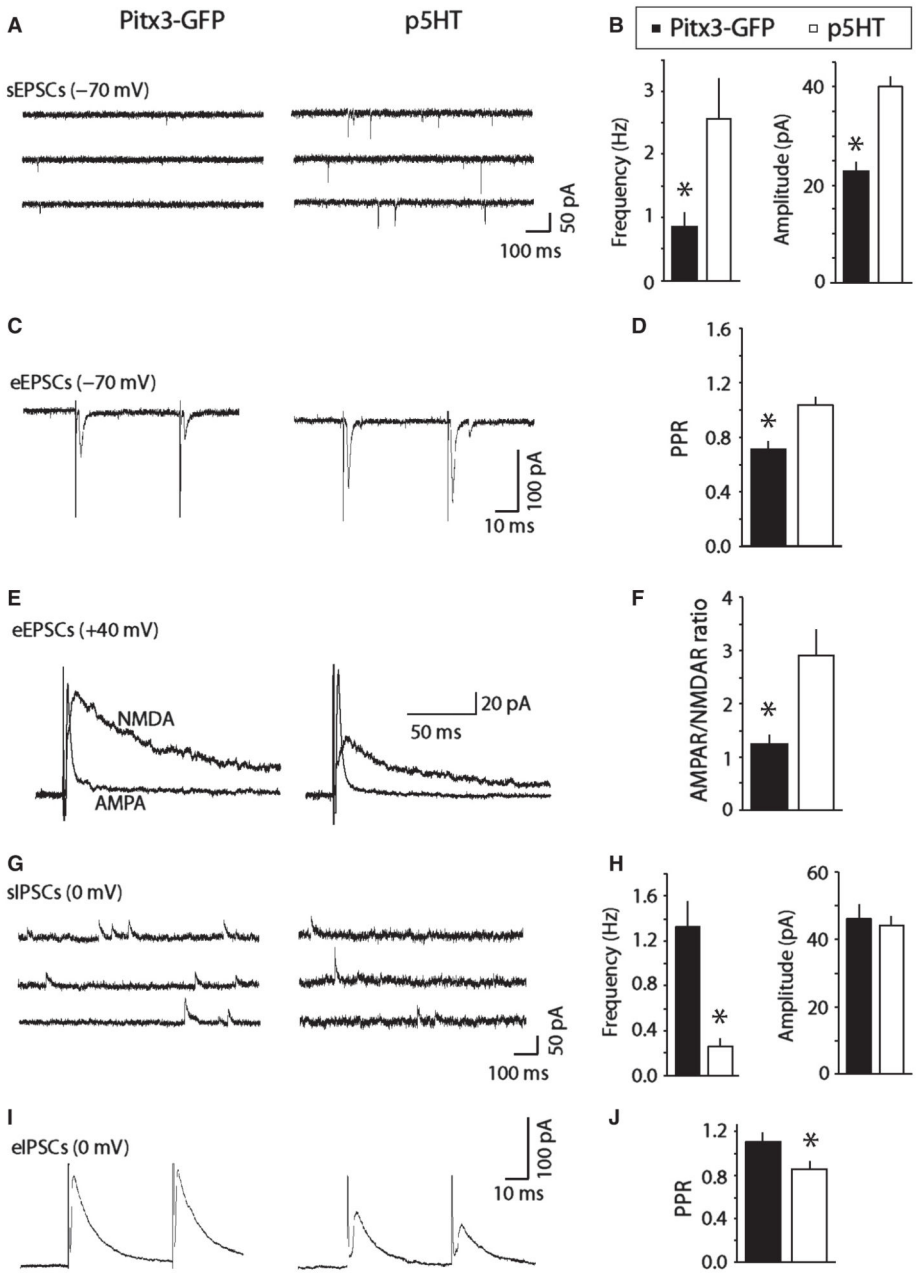

Fig. 5.

DRN/vlPAG dopamine neurons display spontaneous and evoked excitatory glutamatergic and inhibitory GABAergic synaptic activity in brain slices. (A) Examples of spontaneous excitatory synaptic currents (sEPSCs) in Pitx3-GFP+ and p5HT neurons. (B) Bar chart showing average frequency and amplitude of sEPSCs in Pitx3-GFP+ and p5HT neurons. (C) Examples of paired evoked EPSCs (eEPSCs) in Pitx3-GFP+ and p5HT neurons. (D) Bar chart showing average paired-pulse ratios (PPRs) for eEPSCs in Pitx3-GFP+ and p5HT neurons. (E) Examples of evoked AMPA receptor (AMPAR)-mediated synaptic currents, and computed NMDA receptor (NMDAR)-mediated currents (at +40 mV). (F) Bar chart

showing average AMPAR/NMDAR ratios in Pitx3-GFP+ and p5HT neurons. (G). Examples of spontaneous inhibitory synaptic currents (sIPSCs) in Pitx3-GFP+ and p5HT neurons. (H) Bar chart showing average frequency and amplitude of sIPSCs in Pitx3-GFP+ and p5HT neurons. (I) Examples of evoked IPSCs (eIPSCs) in Pitx3-GFP+ and p5HT neurons. (J) Bar chart showing average PPRs for eIPSCs in Pitx3-GFP+ and p5HT. *$P < 0.05$.

Europe PMC Funders Author Manuscripts

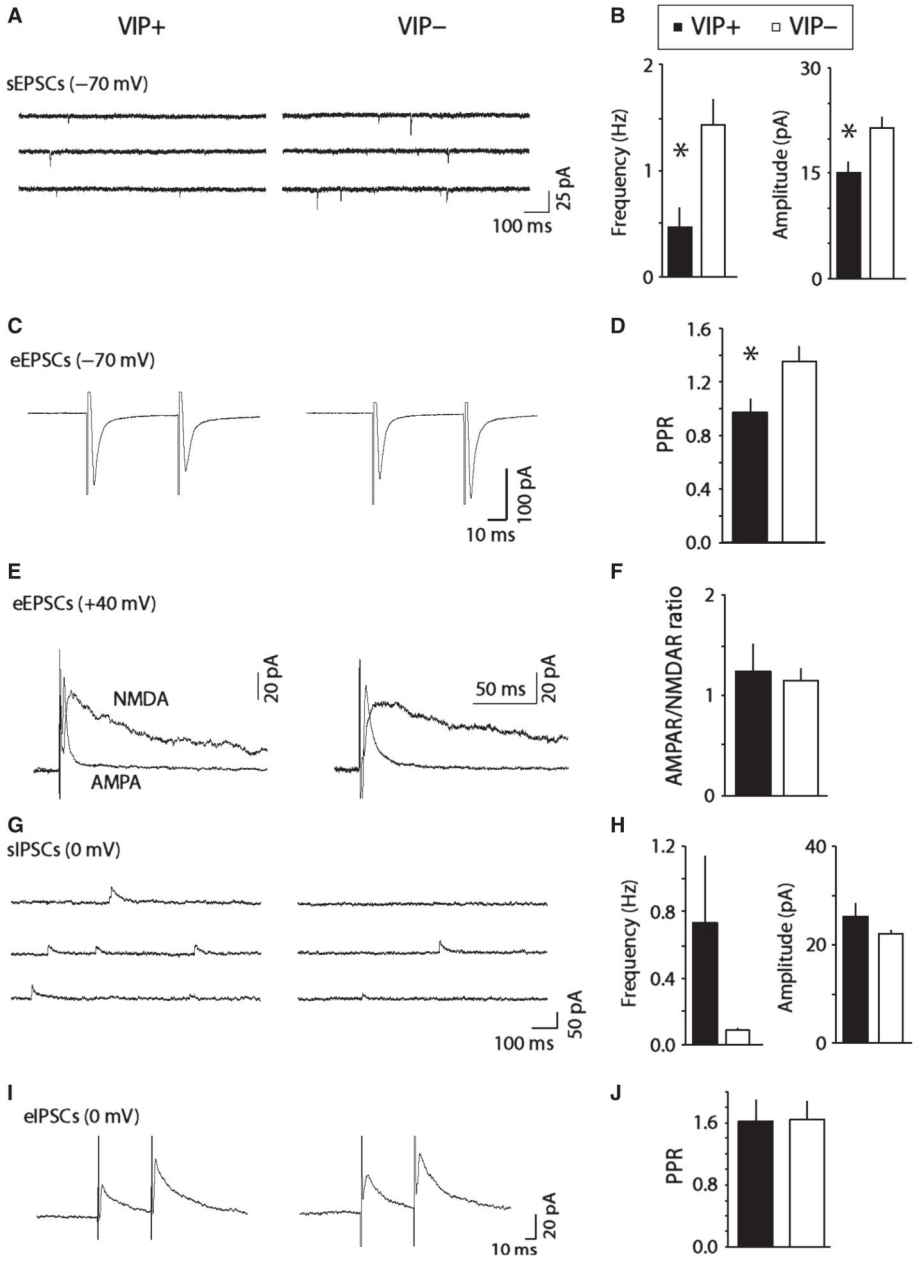

Fig. 6.

Comparison of spontaneous and evoked excitatory glutamatergic and inhibitory GABAergic synaptic activity in VIP+ and VIP− neurons. (A) Examples of spontaneous excitatory synaptic currents (sEPSCs) in VIP+ and VIP− neurons. (B) Bar chart showing average frequency and amplitude of sEPSCs in VIP+ and VIP− neurons. (C) Examples of paired evoked EPSCs (eEPSCs) in VIP+ and VIP− neurons. (D) Bar chart showing average paired-pulse ratios (PPRs) for eEPSCs in VIP+ and VIP− neurons. (E) Examples of evoked AMPA receptor (AMPAR)-mediated synaptic currents, and computed NMDA receptor (NMDAR)-mediated currents (at +40 mV). (F) Bar chart showing average AMPAR/NMDAR ratios in VIP+ and VIP− neurons. (G). Examples of spontaneous inhibitory synaptic currents

(sIPSCs) in VIP+ and VIP− neurons. (H) Bar chart showing average frequency and amplitude of sIPSCs in VIP+ and VIP− neurons. (I) Examples of evoked IPSCs (eIPSCs) in VIP+ and VIP− neurons. (J) Bar chart showing average PPRs for eIPSCs in VIP+ and VIP− neurons. *$P < 0.05$.

Europe PMC Funders Author Manuscripts

Europe PMC Funders Author Manuscripts

Table 1

Firing rate and pattern, and action potential properties (mean ± SEM) for GFP+ subgroup comparisons

Grouping	Pitx3-GFP vs. TH-GFP	TH+ vs. TH−	VIP+ vs. VIP−
***N*=**	**15 vs. 24**	**27 vs. 5**	**15 vs. 18**
Firing rate (Hz)	3.9 ± 0.6 vs. 4.2 ± 0.6	4.3 ± 0.6 vs. 3.6 ± 1.1	3.7 ± 0.8 vs. 4.5 ± 0.7
CV-ISI	0.48 ± 0.14 vs. 0.47 ± 0.07	0.48 ± 0.09 vs. 0.55 ± 0.20	**0.67 ± 0.13 vs. 0.33 ± 0.07**
AP width (ms)	4.3 ± 0.2 vs. 3.9 ± 0.2	4.0 ± 0.2 vs. 4.0 ± 0.5	4.0 ± 0.3 vs. 4.0 ± 0.2
Threshold (mV)	−23.3 ± 2.0 vs. −27.0 ± 1.9	−24.3 ± 1.4 vs. −26.4 ± 0.8	−23.3 ± 2.0 vs. −25.9 ± 1.2
AHP (mV)	−49.0 ± 2.1 vs. −53.0 ± 1.9	−50.8 ± 1.5 vs. −50.5 ± 1.5	−50.7 ± 2.1 vs. −50.8 ± 1.5
AHP rec. rate (mV/ms)	0.11 ± 0.01 vs. 0.13 ± 0.01	0.12 ± 0.01 vs. 0.13 ± 0.01	0.14 ± 0.01 vs. 0.11 ± 0.01

Bold text indicates $P < 0.05$.